

Article

Conductive Polymer (Graphene/PPy)–BiPO₄ Composite Applications in Humidity Sensors

Zhen Zhu ¹, Wang-De Lin ^{2,*}, Zhi-Yi Lin ³, Ming-Hong Chuang ³, Ren-Jang Wu ³ and Murthy Chavali ⁴ 

¹ School of Environmental Science and Safety Engineering, Tianjin University of Technology, Tianjin 300384, China; zhenzhu@tjut.edu.cn

² Department of Center for General Education, St. Mary's Junior College of Medicine Nursing and Management, Yilan 26647, Taiwan

³ Department of Applied Chemistry, Providence University, Taichung 43301, Taiwan; s1063053@gm.pu.edu.tw (Z.-Y.L.); g1096043@gm.pu.edu.tw (M.-H.C.); rjwu@pu.edu.tw (R.-J.W.)

⁴ NTRC-MCETRC and Aarshanano Composite Technologies Pvt. Ltd., Guntur District, Andhra Pradesh 522201, India; Chavalim@gmail.com

* Correspondence: newwander@smc.edu.tw

Abstract: In this particular experiment, a chain of conductive polymer graphene/polypyrrole (Gr/PPy) and BiPO₄—or (Gr/PPy)–BiPO₄—materials were prepared and used as moisture-sensitive materials. The structure and morphology of the conductive polymer (Gr/PPy)–BiPO₄ materials were analyzed using an X-ray diffractometer, scanning electron microscopy, transmission electron microscopy, and energy-dispersive X-ray spectroscopy. Moreover, properties such as hysteresis loop, impedance, sensing response, and response and recovery time were calculated and evaluated using an inductance–capacitance–resistance analyzer. The data expressed that PPy/BiPO₄, as prepared in this study, exhibited excellent sensing properties, with impedance changing by only a few orders of range. Furthermore, the response time and time of recovery were 340 s and 60 s, respectively, and negligible humidity hysteresis occurred at different relative humidities. Therefore, conductive PPy/BiPO₄, as prepared in the present study, is an excellent candidate for application in humidity sensors.

Keywords: graphene; polypyrrole; impedance; BiPO₄; sensing response



Citation: Zhu, Z.; Lin, W.-D.; Lin, Z.-Y.; Chuang, M.-H.; Wu, R.-J.; Chavali, M. Conductive Polymer (Graphene/PPy)–BiPO₄ Composite Applications in Humidity Sensors. *Polymers* **2021**, *13*, 2013. <https://doi.org/10.3390/polym13122013>

Academic Editor: Oh Seok Kwon

Received: 28 May 2021

Accepted: 18 June 2021

Published: 20 June 2021

Publisher's Note: MDPI stays neutral with regard to jurisdictional claims in published maps and institutional affiliations.



Copyright: © 2021 by the authors. Licensee MDPI, Basel, Switzerland. This article is an open access article distributed under the terms and conditions of the Creative Commons Attribution (CC BY) license (<https://creativecommons.org/licenses/by/4.0/>).

1. Introduction

Ambient humidity must be controlled, regulated, and monitored in environments such as dry cabinets, warehouse storage, industrial production, and food processing facilities, as well as in agricultural planting operations, medical diagnostic centers—both facilities in which high-tech instruments are employed—and shelter environments designed for managing life [1,2]. Recently, tremendous scientific effort has been devoted to the detection of environmental humidity. Particularly, many types of humidity sensors have been explored due to their advantages, such as high sensitivity, rapid response and recovery, low hysteresis, and excellent reproducibility. Humidity sensors are commonly classified into capacitive [3,4], resistive [5,6], optical [7,8], bulk acoustic wave [9,10], and quartz crystal microbalance [11,12] humidity sensors. Numerous types of humidity-sensing material have been used for humidity detection. Zhao et al. prepared a SnO₂/MoS₂ hybrid-sensing nanocomposite by synthesis through a two-step hydrothermal route; the sensor with a 5 μm gap had the largest sensitivity at low humidity [13]. Mallick et al. enhanced the humidity-sensing properties of polyvinylidene fluoride titanium dioxide (PVDF-TiO₂) nanocomposites-based capacitive humidity sensors by modifying the film surface of the TiO₂ [14]. Duong et al. fabricated composite multi-walled carbon nanotubes (MWCNTs) and tungsten oxide (WO₃) nanobricks at different mass ratios, which attained a high response with 95 wt.% of MWCNT/WO₃ nanocomposite [15]. Arularasu et al. developed a PVDF/ZnO nanocomposite that was prepared as a humidity sensor through a

simple hydrothermal approach in which the PVDF/ZnO provided more water molecule adsorption and desorption across the humidity sensor surface compared to pure ZnO nanoparticles [16]. Using the cast-drop and evaporation technique, Zebian et al. developed a hydrophilic-sensitive film based on Al₂O₃-PVA that was coated on the surface of no-core fibers; this exhibited high sensitivity to Al₂O₃ [17]. Ye et al. used Fe₃O₄ nanoparticles as an adsorption interface for the concurrent removal of gaseous benzene, toluene, ethylbenzene, m-xylene, and sulfur dioxide at different relative humidities, which indicated high removal efficiencies under dry conditions of Fe₃O₄ [18]. Xie et al. used the complex impedance analysis method to analyze CeO₂ nanoparticles (NPs), which exhibited a rapid and reversible response characterized by a very small hysteresis [19]. Manikandan et al. synthesized nanocrystalline lithium-substituted copper ferrite (Lisingle bond CuFe₂O₄) nanoparticles with a high surface area, and obtained a fast response/recovery time [20]. Manikandan et al. synthesized a nanocrystalline-structured tin-substituted nickel ferrite (Sn-NiFe₂O₄) thin film, which exhibited excellent reproducibility, sensitivity, and response and recovery times [21]. Douani et al. synthesized bismuth ferrite nanoparticles BiFeO₃ and bismuth ferrite/carbon fiber nanocomposites (BFO/CFs) by a hydrothermal process, showing that they have small hysteresis and good stability [22]. Arrizabalaga et al. reported on an accurate interferometric fiber optic humidity sensor of miniature size which showed fast, accurate, and sensitive properties as a commercial capacitive humidity sensor [23]. Hu et al. fabricated a novel, highly stable and sensitive humidity sensor based on bacterial cellulose (BC)-coated quartz crystal microbalance, which exhibited good reversible behavior and good long-term stability [24]. Ko et al. first report all-two-dimensional (2D) bis (trifluoromethane sulfonyl)-amide (TFSA)-doped graphene (GR) (TFSA-GR)/MoS₂/triethylenetetramine (TETA)-doped GR (TETA-GR) vertical-heterostructure semitransparent photodetectors (PDs) on rigid/flexible substrates, which exhibited good stability [25]. Among these, polymers are promising humidity-sensing candidates because they exhibit dramatic changes in electrical conductivity when exposed to various levels of environmental humidity [26–28]; they also have excellent properties, are low-cost to prepare, nontoxic, easy to fabricate, and are stable at room temperature. Additionally, graphene-based humidity sensors have received increased attention because they can generate electricity from the air by absorbing water molecules [29–31].

BiPO₄ is an attractive material to researchers due to its economic cost, chemically stable structure, nontoxicity, photocatalytic characteristics, extraordinary optics, and electronic properties [32,33]. Graphene has attracted much attention from scientists and researchers because of its outstanding advantages, such as high surface area, excellent thermal conductivity, low cost, large-scale synthesis, stability, and electrical and mechanical properties; however, graphene cannot be applied to humidity sensors because of its hydrophobic nature. However, no attempt has been made to construct graphene/polypyrrole (Gr/PPy)-BiPO₄ composite-resistive humidity sensors. In the present research, a series of Gr/PPy-modified BiPO₄ was successfully synthesized, characterized, and investigated as sensing materials for humidity sensors. Moreover, the sensing mechanism, sensing properties, and morphology of as-prepared Gr/PPy-modified BiPO₄ were examined.

2. Experimental Design

2.1. Materials

The 97% pure (Bi(NO₃)₃·5H₂O) bismuth(III)nitrate pentahydrate, trisodium phosphate (Na₃PO₄), pyrrole (C₄H₅N), cetyltrimethylammonium bromide (CTAB), ammonium persulfate (NH₄)₂S₂O₈, and polyvinyl alcohol ((C₂H₄O)_x) were obtained from Sigma-Aldrich Co., Inc. (St. Louis, MO, USA). Graphene was purchased from National Chiayi University in Taiwan. All materials were utilized without any purification. DI water was drawn from a system water purification provided by the Milli-Q system, processed, and used in all experiments.

2.2. Method of Synthesis

As is typical in this procedure, 5 mmol of $\text{Bi}(\text{NO}_3)_3 \cdot 5\text{H}_2\text{O}$ and 2.5 mmol of Na_3PO_4 were dissolved in 46 mL of HNO_3 (0.3 M) under continuous stirring for 1 h to obtain a homogeneous aqueous solution. The resulting solution was transferred into a Teflon-lined stainless steel autoclave. Subsequently, the autoclave was tightly sealed and maintained in a temperature-controlled electric oven at 160 °C for 24 h. Then, after it was filtered and washed with deionized water and ethanol five times, the resulting white product was dried at 70 °C for 12 h to harvest BiPO_4 . Next, an amount of 0.5 g as-prepared BiPO_4 was added to 300 mL of an aqueous solution containing 1% CTAB under ultrasound for 0.5 h to form solution A, whereas solution B was formed by dissolving 0.03 mL of $\text{C}_4\text{H}_5\text{N}$ in solution A under ultrasound for 10 min. Thereafter, 100 mL of 10% $(\text{NH}_4)_2\text{S}_2\text{O}_8$ and solution B were mixed under ultrasound for 0.5 h and maintained under temperatures ranging from 1 °C to 5 °C for 24 h to form a black precipitate. Finally, the as-obtained precipitate was centrifuged, washed with deionized water and ethanol several times, and dried at 70 °C for 2 h to obtain PPy/ BiPO_4 . Additionally, precalculated amounts of as-prepared BiPO_4 and graphene were added to 10 mL of 95% ethanol under ultrasound for 1 h to produce a black suspension. The obtained suspension was centrifuged and washed with ethanol and deionized water and then dried at 60 °C for 12 h to obtain graphene/ BiPO_4 [34–36].

2.3. Characteristic Methods

Structural properties of as-prepared material were analyzed using the powder X-ray diffractometer (XRD) method—the Shimadzu XRD-6000 (operated at 35 kV and 35 mA) with a ($\lambda = 1.5404 \text{ \AA}$) Cu source. The particle size of the as-obtained prepared photocatalysts was averaged and explained using the Debye–Scherrer equation. Transmission electron microscopy (TEM) images were acquired using a JEOL JEM2010 transmission electron microscope (JEOL, Japan) at an accelerating voltage of 200 kV. The samples for TEM analysis were suspended in ethanol with the assistance of ultrasound and dispersed on a copper grid. The chemical composition of the as-synthesized samples was analyzed using an energy-dispersive X-ray spectroscope (EDS). The morphology of different as-prepared materials was observed using field emission scanning electron microscopy (JEOL JSM-7100F, Tokyo, Japan), with the microscope operated at 30 kV.

2.4. Sensor Fabrication and Humidity Testing

A solution of 10% PVA was used as the binder. The sensing chips were fabricated by dip-coating them on a pair of comb-like gold electrodes on an alumina substrate ($10 \times 5 \text{ mm}^2$; rotational speed, 1000 rpm). The chips were subsequently heated at 80 °C for 0.5 h and calcined at 300 °C for 4 h.

The humidity parameter and its response were calculated in a flow system that worked dynamically [37], wherein an airtight glass chamber was developed to preserve the sensors and store them (Figure 1). In the sensor setup, air was injected into the water to generate water vapor, which subsequently filled the testing chamber. Various levels of specific relative humidity (RH) were maintained for 15 min to enable the humidity sources to reach equilibrium. The chamber temperature was controlled at $25 \text{ °C} \pm 2 \text{ °C}$; a thermohygrometer was connected to the testing chamber for RH measurement. Taiwan's Center of Measurement Standard/ITRI provides the standard concentration which was used to calibrate the commercial sensor for humidity. The RH response (S) sensor was calculated as S equals the ratio of R_d and R_h . The parameters of R_d under dry conditions were measured as a value of resistance (12% RH) for the developed sensor, while R_h was measured according to how much resistance would be exerted at a specific humidity [36]. The humidity hysteresis properties were 12% and 90%, and they were then decreased to 12% for the adsorption and desorption of water molecules [38]. $H = \Delta f_{\text{max}}/f_{\text{fs}} \times 100\%$ was evaluated as humidity hysteresis error (H) using the equation provided above, wherein Δf_{max} was the error of hysteresis at its maximum and f_{fs} was the output for the response of the full scale. The response or recovery time was defined as the time required for the impedance

of a sensor to change by 90% of the total impedance, whereas the recovery time was the time required for the reverse process. For dynamic testing, the changes in RH at 12% and 90% were controlled by feeding different ratios of air to water. In the provided experiment setup, a hygrometer (Rotronic) was utilized for measuring the RH value with $\pm 0.1\%$ RH accuracy. Sensing material for the response of impedance against humidity was explained by an analyzer that could measure chemical impedance (DU 6010); the input voltage and frequency were 1 V and 1 kHz, respectively.

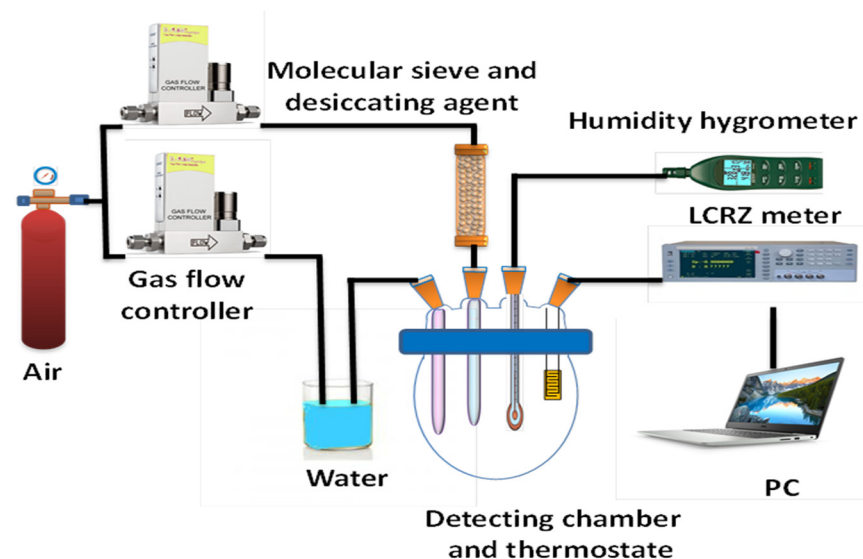


Figure 1. Schematic diagram of the experimental setup.

3. Results and Discussion

3.1. Material Characterizations

To investigate the structural features of the as-fabricated samples, XRD measurement was performed. The XRD patterns of the samples presented in Figure 2 indicate that the main diffraction peak positions were located at the (110), (101), (202), (021), (130), and (040) crystal planes of BiPO_4 , at 2θ values of 21.3° , 23.4° , 27.6° , 41.5° and 50.9° [39], respectively. Additionally, the diffraction peaks were observable at 2θ values of 22.3° and 26.8° , which corresponded to the crystalline planes of PPy and graphene [40,41]. These results indicated that PPy/ BiPO_4 and Gr/ BiPO_4 were successfully synthesized. The diffraction peaks of BiPO_4 with the main lattice plane are (101), (200), (102), and (211) compared to JCPDS, which demonstrate a similar hexagonal phase.

Surface morphology plays an essential role in the humidity-sensing properties of sensing materials, as illustrated in Figure 3a–c. Figure 3a presents polymer diameters roughly in the range of 100 to 150 nanometers for domains in PPy. Figure 3b shows the TEM image of the BiPO_4 (200) lattice plane, which is about 0.329 nm in terms of lattice displacement. TEM images of BiPO_4 are shown at low magnification, at a scale of 100 nm, as well as at a higher magnification. The figure also shows a TEM image of a single BiPO_4 nanorod 569.53 nm in length and 97.92 nm in width. Figure 3c illustrates that leaf-like nanoparticles were uniformly and thinly coated on the surface of the rod-like nanoparticles. Figure 4 suggests that the elemental analysis (EDS) spectrum for PPy/ BiPO_4 indicated the presence of C, O, N, P, and Bi atoms as major components in the as-prepared PPy/ BiPO_4 .

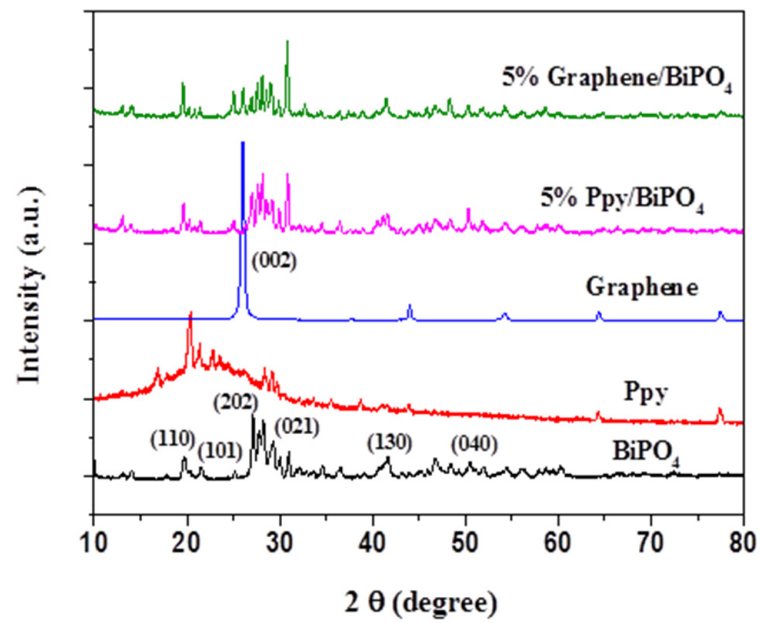


Figure 2. XRD pattern of BiPO₄, PPy, graphene, 5 wt.% PPy/BiPO₄, and 5 wt.% graphene/BiPO₄ composites.

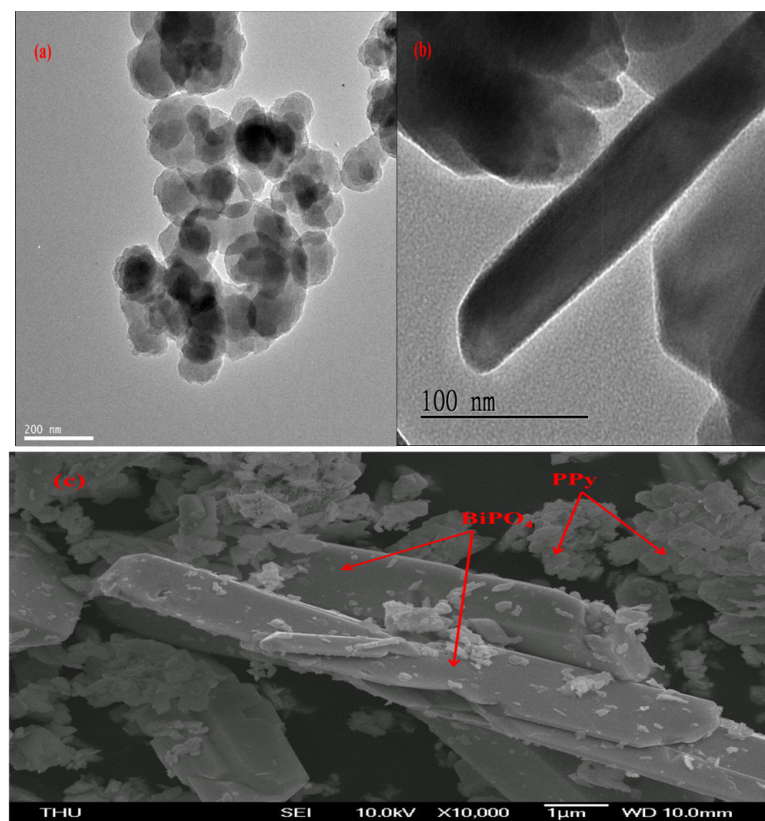


Figure 3. TEM images of (a) PPy, (b) BiPO₄, and (c) FESEM 5 wt.% PPy/BiPO₄ composites.

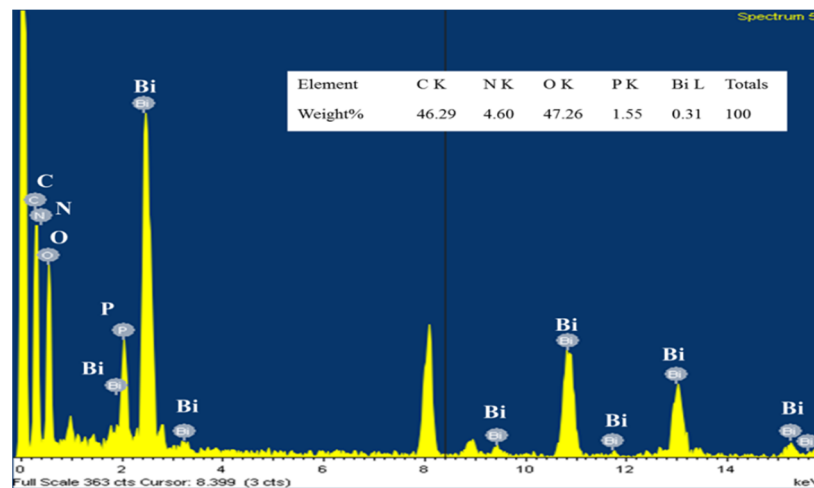


Figure 4. EDX spectrum of the 5 wt.% PPy/BiPO₄ composites.

3.2. Sensing Humidity

The roles of the as-prepared samples in the humidity control were measured and investigated at the optimal operating frequency (1 kHz) (Figure 5). Figure 5 indicates that the impedance values of the as-prepared samples (BiPO₄, PPy, Gr, PPy/BiPO₄, and Gr/BiPO₄) were inversely related to RH changes. Additionally, PPy/BiPO₄ exhibited the most significant change within the RH range, from 12% to 90% (a change of almost three orders of magnitude), suggesting that PPy/BiPO₄ can absorb more water molecules and is thus more sensitive to humidity.

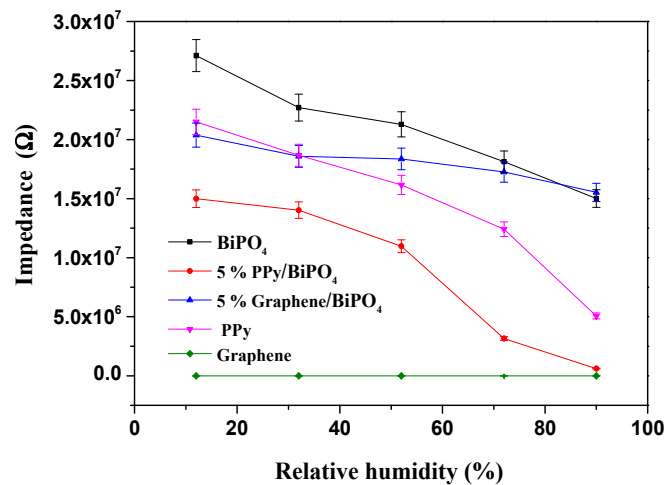


Figure 5. Discrepancies in impedance relative to the variations in relative humidity (%) for varying (Gr/PPy)-BiPO₄ composite contents.

Figure 6a suggests that the response of the as-prepared sample changed gradually with increasing RH under humidity levels lower than 50% RH, whereas the response of the sensor increased sharply with higher ranges of RH. Moreover, PPy/BiPO₄ exhibited the highest humidity in response ($S = 24.6$) to changes in RH (Figure 6).

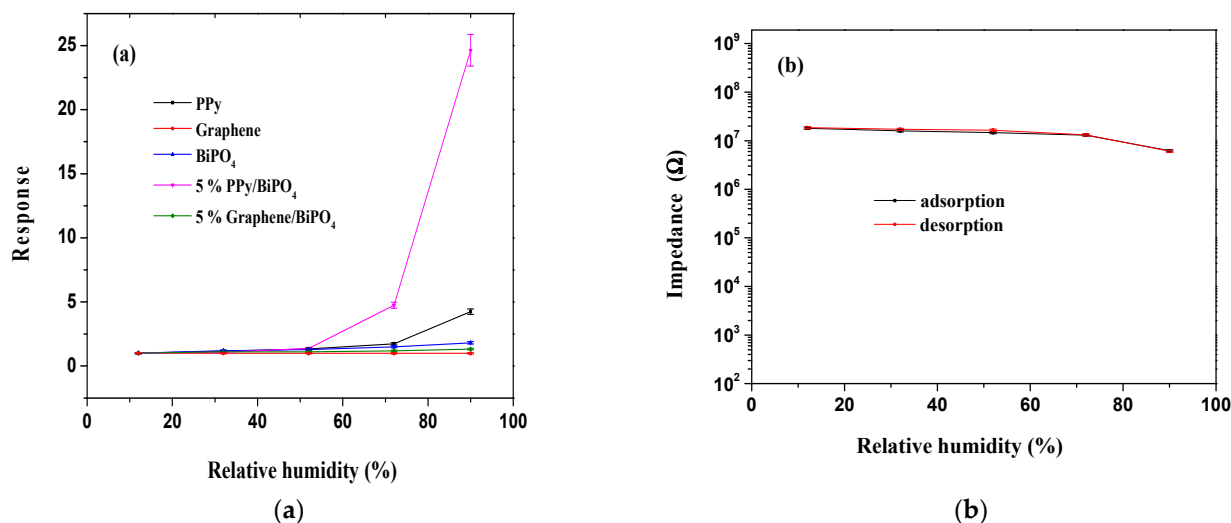


Figure 6. (a) Discrepancies in response relative to the variations in relative humidity (%) for varying (Gr/PPy)-BiPO₄ composite contents; (b) hysteresis characteristics of 5 wt.% PPy/BiPO₄ composite.

Humidity hysteresis, defined as the maximum difference in measured values of RH when the humidity sensor is exposed to adsorption and desorption processes, is an essential parameter for evaluating the reliability of a humidity sensor. Figure 6b suggests that PPy/BiPO₄ had minor humidity hysteresis loss and a relatively large hysteresis loop (0.70%) that occurred at RH levels less than 50%; this indicated that a fast equilibrium could be achieved between the adsorption and desorption process for PPy/BiPO₄.

Crucial parameters such as time of recovery and response data are vital for evaluating the performance of humidity sensors. These parameters represent humidity sensors' speed in measuring RH in various environments. Figure 7 illustrates that the response and recovery times for PPy/BiPO₄ were 340 s and 60 s between 12% RH and 90% RH, respectively. The observed sensing parameters were compared with the previously reported sensors [4,42–45] listed in Table 1. Overall, the PPy/BiPO₄ sensor exhibited an excellent sensing response across the whole humidity range; however, its response and recovery times were longer than those of other sensors, as the PPy/BiPO₄ sensor was tested using materials with different sensitivities. Selectivity is an essential parameter for the practical application of humidity sensors. The cross-sensitivity of PPy/BiPO₄ has been studied for various gases at room temperatures, such as carbon monoxide (CO), ammonia (NH₃), nitrogen dioxide (NO₂), and nitric oxide (NO). As Figure 8 illustrates, the PPy/BiPO₄ sensor had the highest selectivity for humidity and the lowest responsiveness to other types of gases.

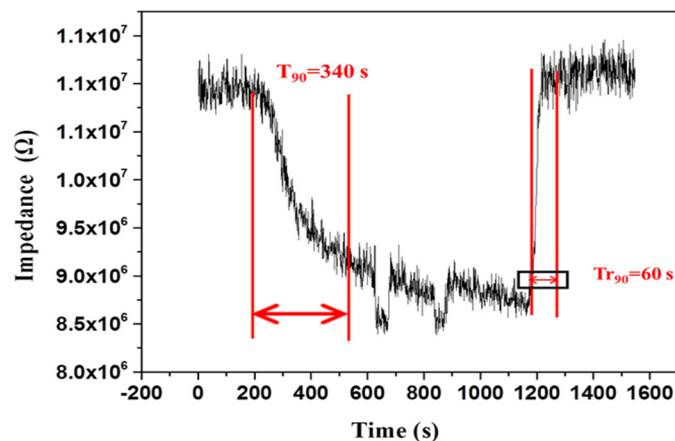
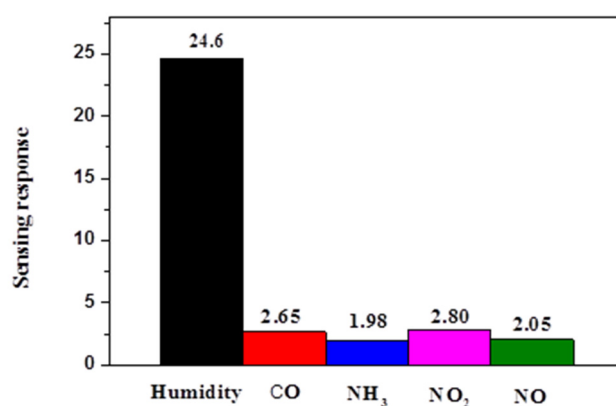


Figure 7. Response and recovery characteristics of 5 wt.% PPy/BiPO₄ composites.

Table 1. Comparative humidity-sensing performance of modified conductive polymer-based sensors with previously published reports.

Sensing Material	Measurement Range (% RH)	Response/Recovery Time (s)	References
MCM-41/PPy	11–95	–915/–100	[42]
RGO/SnO ₂	11–97	102/6	[43]
Trianglamine hydrochloride	5–95	720/300	[44]
MCM-41/PEDOT	11–95	165/115	[4]
PPy	11–95	41/120	[45]
PPy/BiPO ₄	12–90	340/60	This work

**Figure 8.** Selectivity towards relative humidity and various gas species of 5 wt.% PPy/BiPO₄ composites.

3.3. Humidity-Sensing Mechanism

The humidity-sensing mechanism can be explained by the chemical and physical adsorption of water molecules on the PPy/BiPO₄ surface, as illustrated in Figure 9. At low humidity, the probability of contact between water molecules and PPy/BiPO₄ composite was low, so only the outer particles came into contact with the water molecules, as shown in Figure 9a. Since water molecules could not form a continuous water layer in this process, the transfer of H₂O or H₃O⁺ onto the discontinuous water layer was challenging [46]. Therefore, in addition to its use of high-conductor graphene, the sensor impedance is extremely high. Figure 5 shows that, when the RH was 12% in the pure PPy, pure graphene and pure BiPO₄, Gr/BiPO₄, and PPy/BiPO₄ composite, the impedance was $2.15 \times 10^7 \Omega$, $9.18 \times 10^{-1} \Omega$, $2.71 \times 10^7 \Omega$, $2.03 \times 10^7 \Omega$, $1.49 \times 10^7 \Omega$, respectively. As the RH level increased, the physisorption of water molecules occurred on the chemisorbed layer through hydrogen bonding, and the formation of a water multilayer, as illustrated in Figure 9b. The serial water layers accelerated the transfer of H₂O or H₃O⁺. The ion transfer mechanism presented by Grotthuss [47] and Casalbore-Miceli et al. [48] involves the transfer of H₂O or H₃O⁺ on serial water layers $\text{H}_2\text{O} + \text{H}_3\text{O}^+ \rightarrow \text{H}_3\text{O}^+ + \text{H}_2\text{O}$, as shown in Figure 9c. An ionic transfer is the main conduction mode in this process, and the impedance decreases as the relative humidity increases. The rapid transfer of ions on the water layer sharply reduces impedance. The PPy/BiPO₄ composites exhibited humidity-sensing properties that are more favorable than those of the pure PPy or BiPO₄ samples.

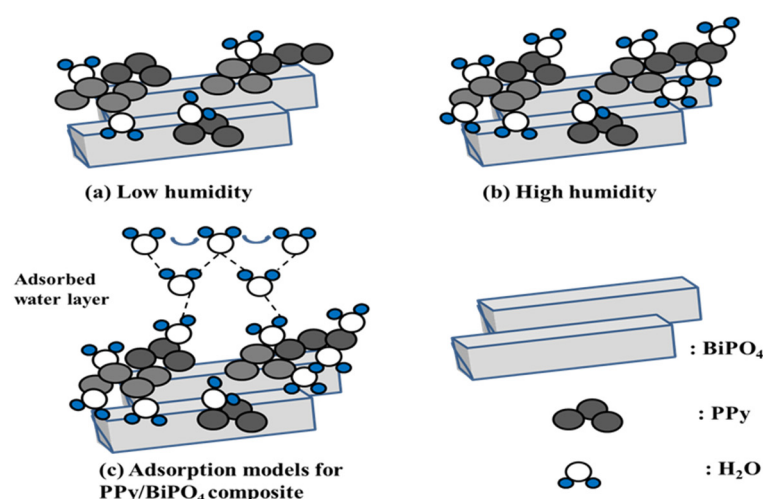


Figure 9. Scheme of humidity-sensing mechanism: (a) low humidity, (b) high humidity, (c) adsorption models for PPy/BiPO₄ composites.

4. Conclusions

In this paper, various polymer (Gr/PPy)–BiPO₄ materials were successfully synthesized and used to detect RH. The structure and morphology samples were characterized by XRD, TEM, FESEM, and EDX. In this study, a humidity sensor based on Gr/BiPO₄ and PPy/BiPO₄ was prepared under room temperature conditions. The experimental results show that the PPy/BiPO₄ composite exhibited excellent humidity-sensing capabilities, including negligible humidity hysteresis, sensing response ($S = 24.6$), and high selectivity. Moreover, the response was 340 s and the recovery time was 30 s. Compared to pure PPy, pure graphene, and pure BiPO₄, as well as Gr/BiPO₄ and PPy/BiPO₄ composites, these results indicate that PPy/BiPO₄-based humidity sensors are good candidates for humidity sensor applications.

Author Contributions: Conceptualization, W.-D.L.; methodology, W.-D.L.; software, W.-D.L.; formal analysis, W.-D.L.; investigation, W.-D.L.; data curation, M.-H.C. and Z.-Y.L.; writing—original draft preparation, Z.Z. and W.-D.L.; writing—review and editing, W.-D.L. and M.C.; visualization, R.-J.W.; project administration, R.-J.W. All authors have read and agreed to the published version of the manuscript.

Funding: This research received no external funding.

Institutional Review Board Statement: Not applicable.

Informed Consent Statement: Not applicable.

Data Availability Statement: Data sharing not applicable.

Acknowledgments: Department of Applied Chemistry is thanked by the authors of Providence University, Sha-Lu, Taichung, for the humidity sensor fabrication.

Conflicts of Interest: The authors declare that they have no known competing financial interests or personal relationships that could have appeared to influence the work reported in this paper.

References

1. Duan, Z.; Jiang, Y.; Yan, M.; Wang, S.; Yuan, Z.; Zhao, Q.; Sun, P.; Xie, G.; Du, X.; Tai, H. Facile, Flexible, Cost-Saving, and Environment-Friendly Paper-Based Humidity Sensor for Multifunctional Applications. *ACS Appl. Mater. Interfaces* **2019**, *11*, 21840–21849. [[CrossRef](#)]
2. Zhang, J.; Wang, X.-X.; Zhang, B.; Ramakrishna, S.; Yu, M.; Ma, J.-W.; Long, Y.-Z. In Situ Assembly of Well-Dispersed Ag Nanoparticles throughout Electrospun Alginate Nanofibers for Monitoring Human Breath—Smart Fabrics. *ACS Appl. Mater. Interfaces* **2018**, *10*, 19863–19870. [[CrossRef](#)] [[PubMed](#)]
3. Ali, S.; Jameel, M.A.; Gupta, A.; Langford, S.J.; Shafiei, M. Capacitive humidity sensing performance of naphthalene diimide derivatives at ambient temperature. *Synth. Met.* **2021**, *275*, 116739. [[CrossRef](#)]

4. Qi, R.; Zhang, T.; Guan, X.; Dai, J.; Liu, S.; Zhao, H.; Fei, T. Capacitive humidity sensors based on mesoporous silica and poly(3,4-ethylene dioxothiophene) composites. *J. Colloid Interface Sci.* **2020**, *565*, 592–600. [[CrossRef](#)] [[PubMed](#)]
5. Ruiz, V.; Fernández, I.; Carrasco, P.; Cabañero, G.; Grande, H.J.; Herrán, J. Graphene quantum dots as a novel sensing material for low-cost resistive and fast-response humidity sensors. *Sens. Actuator B Chem.* **2015**, *218*, 73–77. [[CrossRef](#)]
6. Tang, Q.-Y.; Chan, Y.C.; Zhang, K. Fast response resistive humidity sensitivity of polyimide/multiwall carbon nanotube composite films. *Sens. Actuator B Chem.* **2011**, *152*, 99–106. [[CrossRef](#)]
7. Harith, Z.; Batumalay, M.; Irawati, N.; Harun, S.W.; Arof, H.; Ahmad, H. Relative humidity sensor employing tapered plastic optical fiber coated with seeded Al-doped ZnO. *Optik* **2017**, *144*, 257–262. [[CrossRef](#)]
8. Zhao, Y.; Yuan, Y.; Gan, W.; Yang, M. Optical fiber Fabry–Perot humidity sensor based on polyimide membrane: Sensitivity and adsorption kinetics. *Sens. Actuator A Phys.* **2018**, *281*, 48–54. [[CrossRef](#)]
9. Qiu, X.; Tang, R.; Zhu, J.; Oiler, J.; Yu, C.; Wang, Z.; Yu, H. The effects of temperature, relative humidity and reducing gases on the ultraviolet response of ZnO based film bulk acoustic wave resonator. *Sens. Actuator B Chem.* **2011**, *151*, 360–364. [[CrossRef](#)]
10. Yao, Y.; Xue, Y. Influence of the oxygen content on the humidity sensing properties of functionalized graphene films based on bulk acoustic wave humidity sensors. *Sens. Actuator B Chem.* **2016**, *222*, 755–762. [[CrossRef](#)]
11. Qi, P.; Zhang, T.; Shao, J.; Yang, B.; Fei, T.; Wang, R. A QCM humidity sensor constructed by graphene quantum dots and chitosan composites. *Sens. Actuator A Phys.* **2019**, *287*, 93–101. [[CrossRef](#)]
12. Zhang, D.; Wang, D.; Li, P.; Zhou, X.; Zong, X.; Dong, G. Facile fabrication of high-performance QCM humidity sensor based on layer-by-layer self-assembled polyaniline/graphene oxide nanocomposite film. *Sens. Actuator B Chem.* **2018**, *255*, 1869–1877. [[CrossRef](#)]
13. Zhao, Y.; Yang, B.; Liu, J. Effect of interdigital electrode gap on the performance of SnO₂-modified MoS₂ capacitive humidity sensor. *Sens. Actuator B Chem.* **2018**, *271*, 256–263. [[CrossRef](#)]
14. Mallick, S.; Ahmad, Z.; Touati, F.; Shakoor, R.A. Improvement of humidity sensing properties of PVDF-TiO₂ nanocomposite films using acetone etching. *Sens. Actuator B Chem.* **2019**, *288*, 408–413. [[CrossRef](#)]
15. Duong, V.T.; Nguyen, C.T.; Luong, H.B.; Nguyen, D.C.; Nguyen, H.L. Ultralow-detection limit ammonia gas sensors at room temperature based on MWCNT/WO₃ nanocomposite and effect of humidity. *Solid State Sci.* **2021**, *113*, 106534. [[CrossRef](#)]
16. Arularasu, M.V.; Harb, M.; Vignesh, R.; Rajendran, T.V.; Sundaram, R. PVDF/ZnO hybrid nanocomposite applied as a resistive humidity sensor. *Surf. Interfaces* **2020**, *21*, 100780. [[CrossRef](#)]
17. Zebian, H.Y.; Taher, H.J. Relative humidity sensor based on no-core multimode interferometer coated with Al₂O₃-PVA composite films. *Opt. Fiber Technol.* **2020**, *54*, 102110. [[CrossRef](#)]
18. Ye, C.Z.; Ariya, P.A. Co-adsorption of gaseous benzene, toluene, ethylbenzene, m-xylene (BTEX) and SO₂ on recyclable Fe₃O₄ nanoparticles at 0–101% relative humidities. *J. Environ. Sci.* **2015**, *31*, 164–174. [[CrossRef](#)]
19. Xie, W.; Liu, B.; Xiao, S.; Li, H.; Wang, Y.; Cai, D.; Wang, D.; Wang, L.; Liu, Y.; Li, Q.; et al. High-performance humidity sensors based on CeO₂ nanoparticles. *Sens. Actuator B Chem.* **2015**, *215*, 125–132. [[CrossRef](#)]
20. Manikandan, V.; Sikarwar, S.; Yadav, B.C.; Vigneselvan, S.; Mane, R.S.; Chandrasekaran, J.; Mirzaei, A. Rapid humidity sensing activities of lithium-substituted copper-ferrite (Li–CuFe₂O₄) thin films. *Mater. Chem. Phys.* **2019**, *229*, 448–452. [[CrossRef](#)]
21. Manikandan, V.; Sikarwar, S.; Yadav, B.C.; Mane, R.S. Fabrication of tin substituted nickel ferrite (Sn–NiFe₂O₄) thin film and its application as opto-electronic humidity sensor. *Sens. Actuator A Phys.* **2018**, *272*, 267–273. [[CrossRef](#)]
22. Douani, R.; Lamrani, N.; Oughanem, M.H.; Saidi, M.; Guhel, Y.; Chaouchi, A.; Boudart, B. Improvement of humidity sensing performance of BiFeO₃ nanoparticles-based sensor by the addition of carbon fibers. *Sens. Actuator A Phys.* **2020**, *307*, 111981. [[CrossRef](#)]
23. Arrizabalaga, O.; Velasco, J.; Zubia, J.; Sáez de Ocariz, I.; Villatoro, J. Miniature interferometric humidity sensor based on an off-center polymer cap onto optical fiber facet. *Sens. Actuator B Chem.* **2019**, *297*, 126700. [[CrossRef](#)]
24. Hu, W.; Chen, S.; Zhou, B.; Liu, L.; Ding, B.; Wang, H. Highly stable and sensitive humidity sensors based on quartz crystal microbalance coated with bacterial cellulose membrane. *Sens. Actuator B Chem.* **2011**, *159*, 301–306. [[CrossRef](#)]
25. Ko, J.S.; Shin, D.H.; Lee, W.J.; Jang, C.W.; Kim, S.; Choi, S.-H. All-two-dimensional semitransparent and flexible photodetectors employing graphene/MoS₂/graphene vertical heterostructures. *J. Alloys Compd.* **2021**, *864*, 158118. [[CrossRef](#)]
26. Al-Hayali, S.K.; Salman, A.M.; Hadi Al-Janabi, A. Effect of hygroscopic polymer-coatings on the performance of relative humidity sensor based on macro-bend single-mode fiber. *Opt. Fiber Technol.* **2021**, *62*, 102460. [[CrossRef](#)]
27. Park, Y.-J.; Lee, S.; Kim, B.; Kim, J.-H.; So, J.-H.; Koo, H.-J. Impedance study on humidity dependent conductivity of polymer composites with conductive nanofillers. *Compos. Part B Eng.* **2020**, *202*, 108412. [[CrossRef](#)]
28. Wang, B.; Zhou, J.; Wang, Z.; Mu, S.; Wu, R.; Wang, Z. Cellulose nanocrystal/plant oil polymer composites with hydrophobicity, humidity-sensitivity, and high wet strength. *Carbohydr. Polym.* **2020**, *231*, 115739. [[CrossRef](#)] [[PubMed](#)]
29. Khalifa, M.; Wuzella, G.; Lammer, H.; Mahendran, A.R. Smart paper from graphene-coated cellulose for high-performance humidity and piezoresistive force sensor. *Synth. Met.* **2020**, *266*, 116420. [[CrossRef](#)]
30. Song, Z.; Lin, E.S.; Zhu, J.; Ong, J.W.; Abid, H.A.; Uddin, M.H.; Liew, O.W.; Ng, T.W. Sustained graphene oxide coated superhydrophilicity and superwetting using humidity control. *Colloid Surf. A Physicochem. Eng. Asp.* **2021**, *613*, 126097. [[CrossRef](#)]
31. Zhu, C.; Tao, L.-Q.; Wang, Y.; Zheng, K.; Yu, J.; Li, X.; Chen, X.; Huang, Y. Graphene oxide humidity sensor with laser-induced graphene porous electrodes. *Sens. Actuator B Chem.* **2020**, *325*, 128790. [[CrossRef](#)]

32. Di, J.; Chen, J.; Ji, M.; Zhang, Q.; Xu, L.; Xia, J.; Li, H. Reactable ionic liquid induced homogeneous carbon superdoping of BiPO₄ for superior photocatalytic removal of 4-chlorophenol. *Chem. Eng. J.* **2017**, *313*, 1477–1485. [[CrossRef](#)]
33. Yan, P.; Jiang, D.; Li, H.; Bao, J.; Xu, L.; Qian, J.; Chen, C.; Xia, J. BiPO₄ nanocrystal/BiOCl nanosheet heterojunction as the basis for a photoelectrochemical 4-chlorophenol sensor. *Sens. Actuator B Chem.* **2019**, *279*, 466–475. [[CrossRef](#)]
34. Zhu, Z.; Hong, W.-G.; Chen, C.-Y.; Wu, R.-J. Novel Nanoarchitectonics Olive-Like Pd/BiVO₄ for the Degradation of Gaseous Formaldehyde Under Visible Light Irradiation. *J. Nanosci. Nanotechnol.* **2020**, *20*, 2689–2697. [[CrossRef](#)] [[PubMed](#)]
35. Luk, H.N.; Chen, Y.H.; Hsieh, C.Y.; Han, Y.W.; Wu, R.J.; Chavali, M. A Novel Co₃O₄-BiPO₄ Nanoarchitectonics Material Preparation for the Electrocatalytic Detection of Epinephrine. *J. Nanosci. Nanotechnol.* **2020**, *20*, 2705–2712. [[CrossRef](#)] [[PubMed](#)]
36. Lin, W.-D.; Chang, H.-M.; Wu, R.-J. Applied novel sensing material graphene/polypyrrole for humidity sensor. *Sens. Actuator B Chem.* **2013**, *181*, 326–331. [[CrossRef](#)]
37. Lin, W.-D.; Liao, C.-T.; Chang, T.-C.; Chen, S.-H.; Wu, R.-J. Humidity sensing properties of novel graphene/TiO₂ composites by sol-gel process. *Sens. Actuator B Chem.* **2015**, *209*, 555–561. [[CrossRef](#)]
38. Li, X.; Feng, W.; Zhang, X.; Lin, S.; Chen, Y.; Chen, C.; Chen, S.; Wang, W.; Zhang, Y. Facile fabrication of laser-scribed graphene humidity sensors by a commercial DVD drive. *Sens. Actuator B Chem.* **2020**, *321*, 128483. [[CrossRef](#)]
39. Li, M.; Zhang, G.; Feng, C.; Wu, H.; Mei, H. Highly sensitive detection of chromium (VI) by a photoelectrochemical sensor under visible light based on Bi SPR-promoted BiPO₄/BiOI heterojunction. *Sens. Actuator B Chem.* **2020**, *305*, 127449. [[CrossRef](#)]
40. Alizadeh, T.; Shokri, M. A new humidity sensor based upon graphene quantum dots prepared via carbonization of citric acid. *Sens. Actuator B Chem.* **2016**, *222*, 728–734. [[CrossRef](#)]
41. Kumar, U.; Yadav, B.C.; Haldar, T.; Dixit, C.K.; Yadawa, P.K. Synthesis of MWCNT/PPY nanocomposite using oxidation polymerization method and its employment in sensing such as CO₂ and humidity. *J. Taiwan Inst. Chem. Eng.* **2020**, *113*, 419–427. [[CrossRef](#)]
42. Qi, R.; Lin, X.; Dai, J.; Zhao, H.; Liu, S.; Fei, T.; Zhang, T. Humidity sensors based on MCM-41/polypyrrole hybrid film via in-situ polymerization. *Sens. Actuator B Chem.* **2018**, *277*, 584–590. [[CrossRef](#)]
43. Zhang, D.; Chang, H.; Li, P.; Liu, R.; Xue, Q. Fabrication and characterization of an ultrasensitive humidity sensor based on metal oxide/graphene hybrid nanocomposite. *Sens. Actuator B Chem.* **2016**, *225*, 233–240. [[CrossRef](#)]
44. Chappanda, K.N.; Chaix, A.; Surya, S.G.; Moosa, B.A.; Khashab, N.M.; Salama, K.N. Trianglamine hydrochloride crystals for a highly sensitive and selective humidity sensor. *Sens. Actuator B Chem.* **2019**, *294*, 40–47. [[CrossRef](#)]
45. Sun, A.; Li, Z.; Wei, T.; Li, Y.; Cui, P. Highly sensitive humidity sensor at low humidity based on the quaternized polypyrrole composite film. *Sens. Actuator B Chem.* **2009**, *142*, 197–203. [[CrossRef](#)]
46. Anderson, J.H.; Parks, G.A. Electrical conductivity of silica gel in the presence of adsorbed water. *J. Phys. Chem.* **1968**, *72*, 3662–3668. [[CrossRef](#)]
47. Ernsberger, F.M. The Nonconformist Ion. *J. Am. Ceram. Soc.* **1983**, *66*, 747–750. [[CrossRef](#)]
48. Casalbore-Miceli, G.; Yang, M.J.; Camaioni, N.; Mari, C.M.; Li, Y.; Sun, H.; Ling, M. Investigations on the ion transport mechanism in conducting polymer films. *Solid State Ion* **2000**, *131*, 311–321. [[CrossRef](#)]